Improving Enzyme–Electrode Contacts by Redox Modification of Cofactors

Article *in* Nature · September 1995

DOI: 10.1038/376672a0 · Source: PubMed

5 authors, including:

Evgeny Katz
Clarkson University
450 PUBLICATIONS **28,548** CITATIONS
SEE PROFILE

Achim Stocker
Universität Bern
73 PUBLICATIONS **1,973** CITATIONS
SEE PROFILE

TABLE 2 Properties of the calibrated models of angular velocity

$r_c/R_\odot$	$r_{sh}/R_\odot$	$\Omega_c/2\pi$	$\Omega_{sh}/2\pi$	Deviation	$J_2(\times 10^7)$
0.20	0.20	−0.041		0	1.7
0.25	0.25	0.177		0	1.7
0.20	0.20	0.210		$+1\sigma$	1.7
0.20	0.20	0.724		$+3\sigma$	1.8
0.71	0.71	0.395		0	1.5
0.20	0.45	−0.421	0.576	0	2.4
0.15	0.45	0.600	0.430	$+2\sigma$	1.7
0.71	0.71	0.440		0	1.7

A selection of models of the form illustrated in Fig. 2*a*, fitted by least squares to the mean constant frequency splitting of 0.416 μHz, augmented, where indicated, by the deviation listed in column 5, where $\sigma = 0.009$ μHz. J_2 is the implied quadrupole moment of the external gravitational potential, in the usual units of $GM_\odot R_\odot$, and was computed under the assumption $\Omega = \bar{\Omega}$ for $r < r_e$; in all cases J_2 is consistent with the radar ranging measurements and General Relativity. $M_\odot$ and $R_\odot$ are respectively the mass and radius of the Sun. (The other variables given as column headings are defined in Fig. 2 legend.) The rotation rate of the convection zone is presumed to be given by $\Omega(r, \theta)/2\pi = \Omega_s(\theta)/2\pi = (0.458 - 0.090\cos^2\theta)$μHz, except in row 5, where it is calibrated to be 0.96 $\Omega_s/2\pi = (0.440 - 0.086\cos^2\theta)$μHz and matches onto uniform interior rotation $\Omega_c/2\pi = 0.422$ μHz with continuous latitudinally averaged specific angular momentum. The motivation for that model was the possibility of there being a large-scale poloidal magnetic field causing the radiative interior to rotate rigidly. We have also considered variants of that model in which the angular velocity in the convection zone is $f(r)\Omega_s(\theta)$, where $f(r)$ increases monotonically from a value f_e at the base of the convection zone $r = r_e$ to unity at the photosphere, the value of f_e being such that the specific angular momentum across the interface with the rigidly rotation radiative interior is continuous. In no case was it possible to find a model that reproduced both the splitting data reported here and the inversions of the data from the Big Bear Solar Observatory (BBSO), which are represented as synodic rotation rates in ref. 18. All the seismic data can be reproduced to within 1σ by a model with $\Omega = \Omega_s$ in the convection zone and a radiative interior rotating uniformly at 0.395 ± 0.025 μHz. However, the mean specific angular momentum is no longer continuous at $r = r_e$, suggesting the requirement of a torque. As an example of a different model, one with angular velocity varying linearly in the radiative interior according as $\bar{\Omega} = \Omega_e - (1 - (r/r_e))\Omega_g$ for constant Ω_g satisfies the seismic data with $\Omega_g/2\pi = 116 \pm 57$ nHz, with $\Omega_g/2\pi = 116 \pm 57$ nHz, implying an equatorial angular velocity rather lower than the values inferred by Goode and Dziembowski[22] from the BBSO data in the region $0.4\,R_\odot < r < 0.7\,R_\odot$, and the recent inferences by Tomczyk *et al.*[23] in $0.2R_\odot < r < 0.7\,R_\odot$. For this adjusted linearly varying model, $J_2 = 1.45 \times 10^{-7}$.

Our splitting data force us to conclude that there is a region of significantly slow rotation in the radiative interior of the Sun. As the minimum-energy state is one of uniform rotation, it is likely that the present situation is either transient or perhaps varies with the solar cycle. That might explain why our present results differ from the relatively high splitting reported earlier in refs 4 and 5. Alternatively, the rotation is steady and is maintained by stresses that result from material motion ultimately driven by thermonuclear energy generated in the core. Whether that motion is slow meridional flow, wave motion or simply turbulence in the convection zone whose influence is transmitted by magnetic stresses into the deep interior is an issue that requires further enquiry. □

Received 29 March; accepted 27 July 1995.

1. Snodgrass, H. B. *Solar Phys.* **94,** 13–31 (1984).
2. Christensen-Dalsgaard, J. & Schou, J. *Seismology of the Sun and Sun-like Stars* 149–153 (ESA SP-286 European Space Agency, Noordwijk, 1988).
3. Brown, T. M. *et al. Astrophys. J.* **343,** 526–546 (1989).
4. Claverie, A. *et al. Nature* **293,** 443–445 (1981).
5. Isaak, G. R. *Seismology of the Sun and the Distant Stars* (ed. Gough, D. O.) 275–280 (NATO ASI Ser. C **169,** Reidel, Dordrecht, 1986).
6. Loudagh, S. *et al. Astr. Astrophys.* **275,** L25–L28 (1993).
7. Jiménez, A. *et al. Astrophys. J.* **435,** 874–880 (1994).
8. Toutain, T. & Kosovichev, A. G. *Astr. Astrophys.* **284,** 265–268 (1994).
9. Appourchaux, T. *et al. Astr. Astrophys.* **294,** L13–L16 (1995).
10. Elsworth, Y. *et al. GONG 1994: Helio- and Asteroseismology* (eds Ulrich, R. K., Rhodes, E. J. Jr & Däppen, W.) 43–46 (Conf. Ser. **76,** Astr. Soc. Pacific, San Francisco, 1995).
11. Gough, D. O. & Toomre, J. *A. Rev. Astr. Astrophys.* **29,** 627–684 (1991).
12. Pinsonneault, M. H., Kawaler, S. D., Sofia, S. & Demarque, P. *Astrophys. J.* **338,** 424–452 (1989).
13. Rhodes, E. J. Jr *et al. Astrophys. J.* **351,** 687–700 (1990).
14. Gough, D. O. *Future Missions in Solar, Heliospheric and Space Plasma Physics* 183–197 (ESA SP-235, European Space Agency, Noordwijk, 1985).
15. Dziembowski, W. A. & Goode, P. R. *GONG 1992: Seismic Investigation of the Sun and Stars* (ed. Brown, T. M.) 225–227 (Conf. Ser. 42, Astr. Soc. Pacific, San Francisco, 1993).
16. Brookes, J. R., Isaak, G. R. & van der Raay, H. B. *Mon. Not. R. astr. Soc.* **185,** 1–17 (1978).
17. Elsworth, Y. *et al. Mon. Not. R. astr. Soc.* **265,** 888–898 (1993).
18. Christensen-Dalsgaard, J. *Mon. Not. R. astr. Soc.* **239,** 977–994 (1989).
19. Duvall, T. Jr *et al. Nature* **310,** 22–25 (1984).
20. Cowling, T. G. *Mon. Not. R. astr. Soc.* **101,** 367–373 (1941).
21. Gough, D. O. *et al. Inside the Stars* (eds Weiss, W. W. & Baglin, A.) 93–96 (Conf. Ser. **40,** Astr. Soc. Pacific, San Francisco, 1993).
22. Goode, P. R. & Dziembowsi, W. A. *GONG 1992: Seismic Investigation of the Sun and Stars* (ed. Brown, T. M.) 217 (Conf. Ser. **42,** Astr. Soc. Pacific, San Francisco, 1993).
23. Tomczyk, S., Schou, J. & Thompson, M. J. *Astrophys. J. Lett.* (in the press).
24. Elsworth, Y. *et al. Mon. Not. R. astr. Soc.* **242,** 135–140 (1990).

SUPPLEMENTARY INFORMATION. Requests should be addressed to Mary Sheehan at the London editorial office of *Nature*.

ACKNOWLEDGEMENTS. We thank all members, past and present, of the solar groups at Birmingham and the Instituto de Astrofisica de Canarias for their assistance; the staff at the South African Astronomical Observatory (SAAO), the Carnegie Institution of Washington, the Australia Telescope, CSIRO, Australia, and E. J. Rhodes Jr for their hospitality at our Sutherland, Las Campanas, Narrabri and Mount Wilson sites, respectively; P. Fourie for technical help; T. Sekii for assistance with computations; and R. S. Stobie for the facilities of SAAO. We thank PPARC for support.

Improving enzyme–electrode contacts by redox modification of cofactors

Azalia Riklin*, Eugenii Katz*, Itamar Willner*†, Achim Stocker‡ & Andreas F. Bückmann‡

* Institute of Chemistry, The Hebrew University of Jerusalem, Jerusalem 91904, Israel
‡ Gesellschaft für Biotechnologische Forschung, Department of Enzymology, Mascheroder Weg 1, D-38124 Braunschweig, Germany

EFFICIENT electron transfer of redox proteins to and from their environment is essential for the use of such proteins in biotechnological applications such as amperometric biosensors and photosynthetic biocatalysts[1–3]. But most redox enzymes lack pathways that can transport an electron from their embedded redox site to an electrode[4,5] or a diffusing photoexcited species[6]. Electrical communication between redox proteins and electrode surfaces has been improved by aligning proteins on chemically modified electrodes[7–9], by attaching electron-transporting groups[10,11] and by immobilizing proteins in polymer matrices tethered by redox groups[12–14]. Generally these methods involve contacting the enzymes at random with electron relay units. Here we report an approach that allows site-specific positioning of electron-mediating units in redox proteins. We strip glucose oxidase of its flavin adenine dinucleotide (FAD) cofactors, modify the latter with redox-active ferrocene-containing groups, and then reconstitute the apoprotein with these modified cofactors. In this way, electrical contact between an electrode and the resulting enzyme in solution is greatly enhanced in a controlled and reproducible way.

The apoprotein originating from glucose oxidase (from *Aspergillus niger*, EC 1.1.3.4), was prepared by acidification of an enzyme solution to pH 1.7, followed by separation on a Sephadex G-25 column and further purification with charcoal–dextran[15]. N^6-(2-aminoethyl)-FAD (compound **1**; Fig. 1)[16] was reacted with *N*-(2-methylferrocene)caproic acid, (**2**)[17], in the presence of 1-ethyl-3-(3-dimethylaminopropyl)carbodiimide, EDC, to yield the ferrocene-modified FAD analogue N^6-[*N*-(2-methylferrocene)-caproylamidoethyl]-FAD (**3**). Glucose

† To whom correspondence should be addressed.

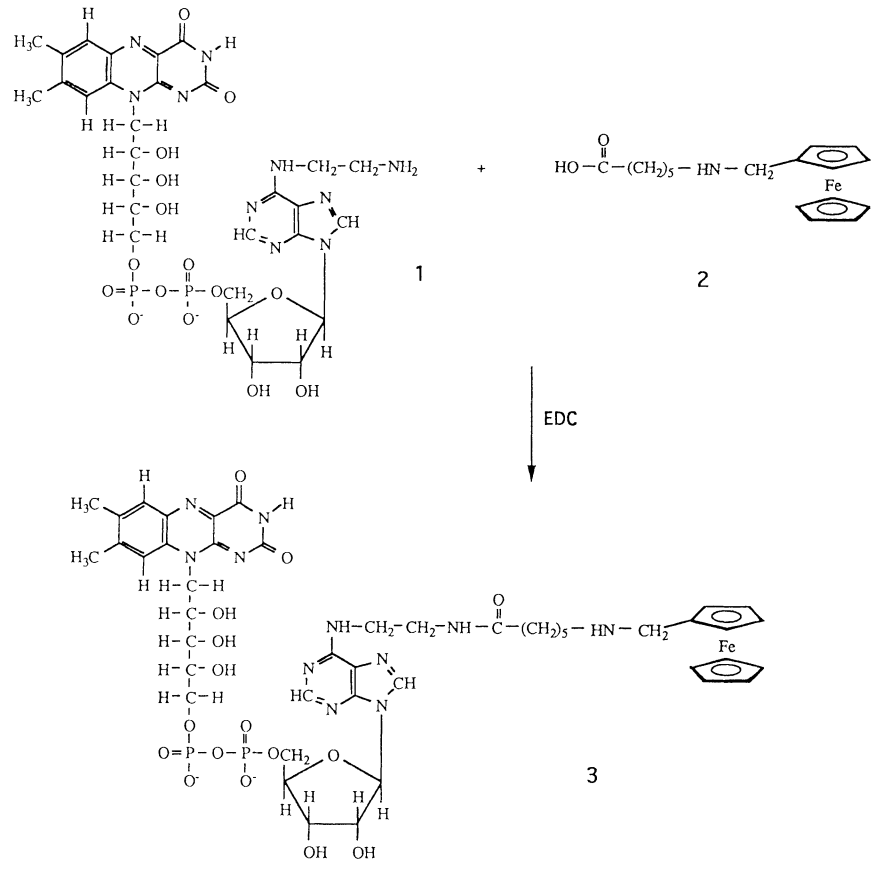

FIG. 1 Structures of compounds **1**, **2** and **3**. EDC is 1-ethyl-3-(3-dimethyl-aminopropyl) carbodiimide.

oxidase apoprotein was reacted with **3** (in the molar ratio 1:10) to generate the ferrocene-FAD reconstituted glucose oxidase. The loading of the reconstituted enzyme was determined spectroscopically as one molecule of **3** per enzyme subunit. Figure 2 shows the cyclic voltammogram of **3** and of the ferrocene-modified-FAD reconstituted glucose oxidase. The ferrocene-FAD analogue (**3**) exhibits, in an aqueous buffer solution at pH 7.3, two characteristic reversible waves at −0.50 and 0.35 V (with respect to the saturated calomel electrode, SCE). These waves correspond to the two-electron redox process of FAD and the one-electron redox reaction of the ferrocene, respectively. The cyclic voltammogram of **3**-reconstituted glucose oxidase shows only the reversible redox process of the ferrocene unit, implying that the ferrocene component communicates with the electrode where the enzyme-embedded FAD component lacks direct electrical communication with the electrode. Enzymatic assay of the original glucose oxidase apoprotein and the **3**-reconstituted glucose oxidase—using the standard procedure of following the H_2O_2 generated by oxidation of glucose using peroxidase and dianisidine as indicator—revealed that the apoenzyme lacks any biocatalytic activity, whereas the reconstituted enzyme has ~60% of the native glucose oxidase activity.

Figure 3*a* shows the electrocatalytic anodic currents developed by the **3**-reconstituted glucose oxidase in the presence of different concentrations of added glucose. A gold foil working electrode (area, 0.4 cm^2; roughness factor, 1.2), precoated with cystamine monolayer, was employed to prevent non-specific, denaturing, enzyme adsorption on the metal surface. The electrocatalytic anodic current is enhanced as the glucose concentration is increased, and reaches a saturation value. The calibration curve, showing the anodic current at different glucose concentrations, is given in Fig. 3*b*. The electrobiocatalysed oxidation of glucose can be analysed in terms of the Michaelis–Menten model, Fig. 3*c*, giving $I_{max} = 4$ μA and $K_m = 2.9$ mM, where I_{max} is the saturation current and K_m is the Michaelis–Menten constant. Taking into account the surface area and roughness factor of the working electrode, this maximum current density corresponds to $i_{max} = 8.3$ μA cm^{-2}. For comparison, native glucose oxidase, under comparable conditions in the presence of ferrocene carboxylic acid, yields the values $K_m = 3.3$ mM and $i_{max} = 6.3$ μA cm^{-2}. We conclude that reconstitution of glucose oxidase with the ferrocene-modified-FAD cofactor (**3**) yields a semisynthetic electroenzyme exhibiting electrical communication between the electrode and the biocatalyst active site.

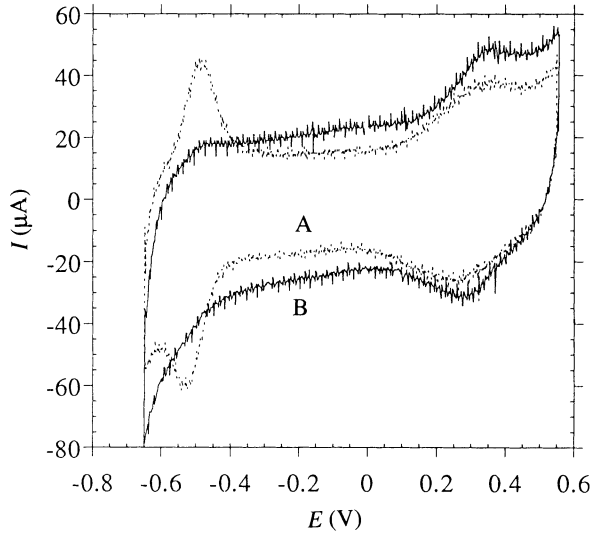

FIG. 2 Cyclic voltammograms. Trace A, ferrocene-modified-FAD analogue (**3**) adsorbed onto a gold working electrode from a 1×10^{-5} M stock solution. Trace B, **3**-reconstituted glucose oxidase, in solution (1.75 mg ml^{-1}) using a cystamine monolayer-modified Au^- electrode. Electrolyte solution; 0.1 M phosphate buffer, pH 7.3. Voltages measured with respect to SCE; scan rate, 1.5 V s^{-1}.

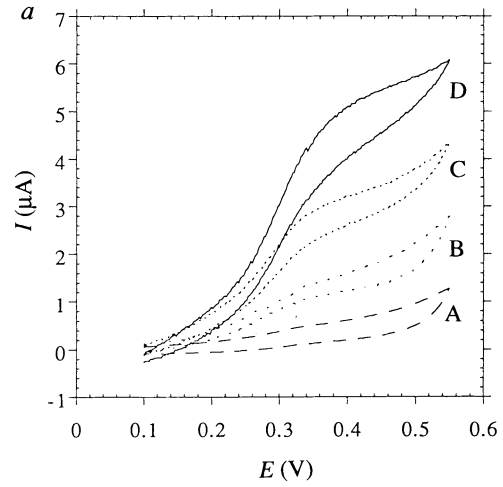

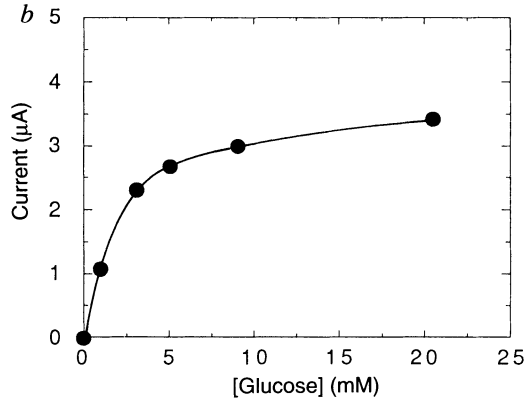

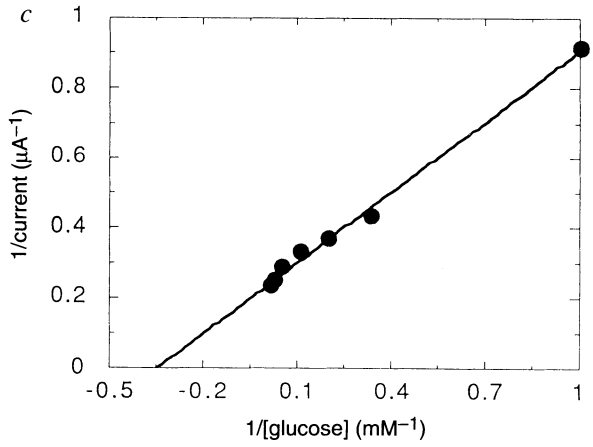

FIG. 3 *a*, Cyclic voltammograms of systems that contain **3**-reconstituted glucose oxidase, 1.75 mg ml^{-1}, and different concentrations of glucose: trace A, 0 mM; B, 1 mM; C. 3 mM; D, 20.5 mM. All experiments were performed in 0.1 M phosphate buffer, pH 7.3, at 35 ± 0.5 °C, using a gold working electrode. Voltages measured with respect to SCE; scan rate, 2 mV s^{-1}. *b*, Calibration curve of electrocatalytic anodic currents at different glucose concentrations in the presence of **3**-reconstituted glucose oxidase. *c*, Lineweaver–Burk plot of the electrobiocatalytic oxidation of glucose by **3**-reconstituted glucose oxidase.

Several control experiments were performed to support the direct electrical communication between the reconstituted enzyme and the electrode. If compound **3** dissolved in an aqueous buffer solution at pH 7.3) undergoes a similar procedure to that employed in the reconsitution—involving filtration through a cut-off filter followed by dialysis—a solution is generated that lacks any electrochemical response by itself or in the presence of native glucose oxidase and glucose as substrate. Also, the **3**-reconstituted enzyme revealed, after chromatographic elution through Sephadex-G25, a similar electrocatalytic activity as observed after reconstitution. Thus any diffusional electrical communication of the reconstituted enzyme through an impurity of **3** is eliminated. Therefore, **3**-reconstituted glucose oxidase represents an organized enzyme assembly exhibiting effective electrical communication with the electrode surface.

The apoprotein derived from D-aminoacid oxidase (DAAO; from pig kidney, EC 1.4.3.3) was prepared[18] as follows. The enzyme was dialysed against a 0.1 M pyrophosphate buffer solution (pH 8.5, containing 1 M KBr and 3×10^{-3} M EDTA), followed by dialysis against a 0.1 M pyrophosphate buffer (pH 8.5). The resulting DAAO apoprotein was reconstituted with **3** by mixing the protein and **3** at a 1:5 molar ratio in a 0.1 M pyrophosphate buffer solution (pH 8.5), followed by filtration through a protein cut-off filter and dialysis against the buffer.

The loading of **3** in the reconstituted DAAO corresponds to one ferrocene-FAD analogue per enzyme. Enzymatic assay showed that the reconstituted enzyme exhibits 20% of the native DAAO activity. (The assay involved the analysis of H_2O_2 formed on biocatalysed oxidation of D-alanine by molecular oxygen, using peroxidase and dianisidine as indicator.) The reconstituted DAAO showed electrical communication with electrode surfaces, and electrocatalytic anodic currents were observed in the presence of D-alanine as substrate. Figure 4 shows the cyclic voltammograms observed on addition of different concentrations of D-alanine to a pH 8.5 electrolyte solution that contains **3**-reconstituted DAAO. The electrocatalytic anodic current is enhanced as the concentration of D-alanine increases. The respective calibration curve was similarly analysed in terms of the Michaelis–Menten model, and the values $I_{max} = 1.9$ μA (or $i_{max} = 3.96$ μA cm^{-2}) and $K_m = 2$ mM were derived for the semi-synthetic electroactive DAAO. Similar to the reconstituted glucose oxidase system, all of the control experiments confirm direct electrical communication between the electrode and the ferrocene-modified-FAD reconstituted DAAO.

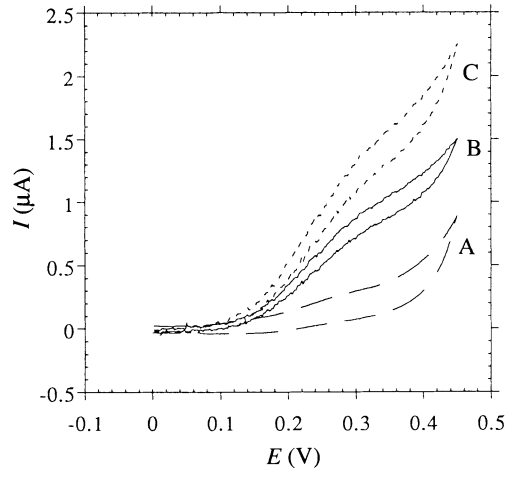

FIG. 4 Cyclic voltammograms of **3**-reconstituted DAAO, 0.38 mg ml^{-1} in the presence of D-alanine: trace A, 0 mM; B, 2 mM; C, 9 mM. Experiment recorded in 0.1 M pyrophosphate buffer, pH 8.5, 25 ± 0.5 °C, using a 0.4-cm^2 gold working electrode, roughness factor 1.2. Voltages measured with respect to SCE; scan rate, 2 mV s^{-1}.

We thus conclude that reconstitution of flavoenzymes by a synthetic ferrocene-tethered FAD cofactor provides a means to generate a new class of electroactive biocatalysts for possible use in amperometric biosensors. The structurally defined adducts formed on reconstitution will be suitable for the elucidation of structure–function relations with respect to electrocatalytic activities of flavoenzymes. □

Received 5 May; accepted 27 July 1995.

1. Blum, L. J. & Coulet, P. R. (eds) *Biosensors, Principles and Applications* (Dekker, New York, 1991).
2. Buck, R. P., Hatfield, W. E., Umana, M. & Bowden, E. F. (eds) *Biosensor Technology Fundamentals and Applications* (Dekker, New York, 1990).
3. Willner, I. & Willner, B. in *Topics in Current Chemistry, Photoinduced Electron Transfer III* Vol. 159 (ed. Mattay, J.). 153 (Springer, Berlin, 1991).
4. Heller, A. *Accts chem. Res.* **23,** 128–134 (1990).
5. Heller, A. *J. phys. Chem.* **96,** 3579–3587 (1992).
6. Willner, I. *et al. J. Am. chem. Soc.* **116,** 1428–1441 (1994).
7. Armstrong, F. A., Hill, H. A. O. & Walton, N. J. *Accts chem. Res.* **21,** 407–413 (1988).
8. Lion-Dagan, M., Katz, E. & Willner, I. *J. chem. Soc., chem. Commun.* 2741–2742 (1994).
9. Gorton, L. *et al. Analyst* **117,** 1235–1241 (1992).
10. Dagani, Y. & Heller, A. *J. Am. chem. Soc.* **110,** 2615–2620 (1988).
11. Schuhmann, W., Ohara, T. J., Schmidt, H.-L. & Heller, A. *J. Am. chem. Soc.* **113,** 1394–1397 (1991).
12. Degani, Y. & Heller, A. *J. Am. chem. Soc.* **111,** 2357–2358 (1989).
13. Foulds, N. C. & Lowe, C. R. *Analyt. Chem.* **60,** 2473–2478 (1988).
14. Willner, I., Katz, E., Lapidot, N. & Bäuerle, P. *Bioelectrochem. Bioenerg.* **29,** 29–45 (1992).
15. Morris, D. L. & Buckler, R. T. in *Methods in Enzymology* Vol. 92, Part E (eds Langone, J. J. & Van Vunakis, H.) 415–417 (Academic, New York, 1983).
16. Bückmann, A. F., Erdmann, H., Pietzsch, M., Hall, J. M. & Bannister, J. V. in *Flavins and Flavoproteins* (ed. Kuneoyagi, K.) 597 (Gruyter, Berlin, 1994).
17. Willner, I., Riklin, A., Shoham, B. Rivenson, D. & Katz, E. *Adv. Mater.* **5,** 912–915 (1993).
18. Massey, V. & Curti, B. *J. biol. Chem.* **241,** 3417–3423 (1966).

ACKNOWLEDGEMENTS. This work was supported by the Ministry of Science of Technology, Israel, and the Commission of the European Communities.

Forest-killing diffuse CO_2 emission at Mammoth Mountain as a sign of magmatic unrest

C. D. Farrar*, M. L. Sorey†, W. C. Evans†, J. F. Howle*, B. D. Kerr‡, B. M. Kennedy§, C.-Y. King† & J. R. Southon‖

* US Geological Survey, Carnelian Bay, California 96140, USA
† US Geological Survey, Menlo Park, California 94025, USA
‡ US Geological Survey, Sacramento, California 95825, USA
§ Lawrence Berkeley National Laboratory, Berkeley, California 94720, USA
‖ Lawrence Livermore National Laboratory, Livermore, California 94551, USA

Mammoth Mountain, in the western United States, is a large dacitic volcano with a long history of volcanism that began 200 kyr ago[1] and produced phreatic eruptions as recently as 500 ± 200 yr BP (ref. 2). Seismicity, ground deformation and changes in fumarole gas composition suggested an episode of shallow dyke intrusion in 1989–90 (refs 3, 4). Areas of dying forest and incidents of near asphyxia in confined spaces, first reported in 1990, prompted us to search for diffuse flank emissions of magmatic CO_2, as have been described at Mount Etna[5] and Vulcano[6]. Here we report the results of a soil-gas survey, begun in 1994, that revealed CO_2 concentrations of 30–96% in a 30-hectare region of killed trees, from which we estimate a total CO_2 flux of ⩾1,200 tonnes per day. The forest die-off is the most conspicuous surface manifestation of magmatic processes at Mammoth Mountain, which hosts only weak fumarolic vents and no summit activity. Although the onset of tree kill coincided with the episode of shallow dyke intrusion, the magnitude and duration of the CO_2 flux indicates that a larger, deeper magma source and/or a large reservoir of high-pressure gas is being tapped.

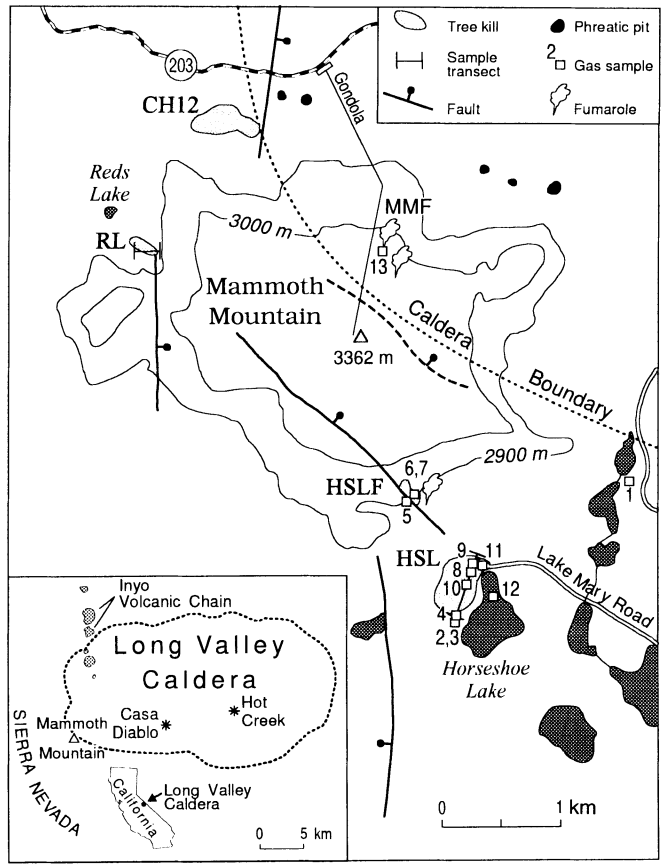

FIG. 1 Maps of Mammoth Mountain and Long Valley caldera showing four areas (light shading) of anomalous tree-kill (labelled HSL, HSLF, RL and CH12), including two transects (RL and HSL) along which [CO_2] has been measured at 0.6 m depth (Fig. 2). Analyses of gas sampled at numbered sites are given in Table 1. Tree line generally follows 3,000 m topographic contour. Also shown are three weak thermal areas with fumaroles at or below boiling temperatures, including the MMF vent that showed increased $^3He/^4He$ values beginning in 1989 (ref. 3). Inset, map of the 760-kyr-old Long Valley caldera showing Mammoth Mountain at the southern terminus of the Inyo Craters volcanic chain, a north-trending set of domes and phreatic explosion craters dated at 40 kyr to 550 yr BP (refs 1, 2).

Mammoth Mountain lies on the southwestern rim of the 760-kyr-old Long Valley caldera in eastern California (Fig. 1). Areas of tree kill on the flanks of Mammoth Mountain were initially considered to be an effect of four years of persistent drought. But it was later noted that all trees, regardless of age or species, were equally affected within dead or dying areas which gradually increased in number and size. Forest Service biologists eventually determined that biological pests were not the cause of the tree kill (F. Richter, personal communication). In July 1994, we made reconnaissance soil-gas surveys in three tree-kill areas and found that samples from 15 cm depth contained >20% CO_2.

In September and October 1994, we collected ~100 soil-gas samples at 30–60 cm depths within tree-kill areas and from control sites in healthy forest. Carbon dioxide concentrations ([CO_2], vol.%) analysed by a portable gas chromatograph ranged from <1% in healthy forest to >90% at several locations within tree-kill areas. Where [CO_2] exceeded 30%, most trees were dead (Fig. 2). Other lethal agents are not apparent. Results from analyses of a subset of soil-gas samples are summarized in Table 1. Sulphur gas concentrations were indistinguishable from background. High temperatures (to 90 °C) and acidic conditions (but without CO_2) have become prevalent in the soil around a geothermal power plant at Casa Diablo (Fig. 1), where ~20 ha of trees have been killed. In the Mammoth Mountain tree-kill